Journal of Magnetic Resonance 294 (2018) 83–92

Contents lists available at ScienceDirect

Journal of Magnetic Resonance

journal homepage: www.elsevier.com/locate/jmr

Engineering spin Hamiltonians using multiple pulse sequences in solid state NMR spectroscopy

Jiangyu Cui [a,d], Jun Li [b], Xiaomei Liu [a,d], Xinhua Peng [a,c,d,*], Riqiang Fu [e,*]

[a] CAS Key Laboratory of Microscale Magnetic Resonance and Department of Modern Physics, University of Science and Technology of China, Hefei 230026, China
[b] Institute for Quantum Science and Engineering, Southern University of Science and Technology, Shenzhen 518055, China
[c] Synergetic Innovation Center for Quantum Effects and Applications, Hunan Normal University, Changsha 410081, China
[d] Synergetic Innovation Center of Quantum Information and Quantum Physics, University of Science and Technology of China, Hefei, Anhui 230026, China
[e] National High Magnetic Field Lab, 1800 East Paul Dirac Drive, Tallahassee, FL 32310, USA

ARTICLE INFO

Article history:
Received 14 April 2018
Revised 19 June 2018
Accepted 22 June 2018
Available online 23 June 2018

Keywords:
Solid-state NMR
Average Hamiltonian theory
Homonuclear decoupling
Multiple pulses
Heteronuclear correlation

ABSTRACT

Multiple pulse sequences are often used to manipulate spin Hamiltonians in solid-state nuclear magnetic resonance spectroscopy. In this paper, we analyze multiple pulse sequences using the well-known average Hamiltonian theory. We first expand the resulting average Hamiltonian into a reachable set of sub-Hamiltonians and then develop a general procedure using both flip-angle and phase of the applied pulses as control variables to select any of those sub-Hamiltonians. We use this method to analyze solid-echo based sequences and to design new proton-proton homonuclear decoupling sequences in static solids. It is found that this newly designed decoupling scheme, in the presence of finite pulse length, effectively suppresses the ^{1}H–^{1}H homonuclear dipolar interactions while establishes variable scaling factors on the heteronuclear dipolar interactions and chemical shift interactions, depending on the flip-angle of the applied pulses. When the pulse flip-angle is close to 54.7°, this sequence possesses a large scaling factor with relatively low average decoupling field. When the pulse flip-angle becomes ~120°, the scaling factor is almost zero. A static ^{15}N-acetyl-valine crystal sample has been used as an example to confirm and validate the performance of this new decoupling scheme.

© 2018 Elsevier Inc. All rights reserved.

1. Introduction

Since the earliest development of nuclear magnetic resonance (NMR), multiple pulse techniques have been commonly used in numerous experiments. In the first multiple pulse experiment, two pulse Hahn-echo [1] was put forward to remove the effect of inhomogeneity in static magnetic field in 1950, while three pulse echoes and Carr-Purcell sequence [2] were the first cyclic multiple pulse experiment. Although these pulse sequences were first applied to solution samples, it was soon found that similar pulse sequences could be applied to solids, capable of achieving high resolution spectra in solid-state NMR. Later on a series of multiple pulse sequences were designed for homonuclear decoupling [3–6], heteronuclear decoupling [7,8] and multiple quantum excitation [9] in solid-state NMR. Behind the techniques is the average Hamiltonian theory (AHT) developed by Haeberlen and Waugh [10] which is a proven powerful theoretical framework for analyzing multiple-pulse sequences in solid-state NMR [5,6,11]. Designing valid multiple pulse sequences has continued to be an important topic, and many relevant methods based on symmetry have been proposed [8,12,13]. In principle, any external perturbations, either in the spin space through multiple pulses or in the laboratory frame via sample spinning, can manipulate the spin Hamiltonians [14]. A fundamental issue in designing multiple pulse sequences in the spin space is to select a specific spin Hamiltonian of interest, while suppressing any other Hamiltonians. This would allow us to simplify the spin system in order to obtain useful spectroscopic information. The ability to selectively average out undesired interactions while at the same time to retain those interactions of interest is particularly important in NMR quantum computation and simulation [15], as it is related to the controllability problem of the system. Liquid-state NMR has been recognized as a well-established small-sized qubit quantum information processor to implement the quantum logic gates and simulate quantum dynamics [16–21]. Due to the complexity of the Hamiltonian and the indistinguishability of nuclear spins in solid-state NMR, it is more challenging to selectively control the Hamiltonian in solids.

* Corresponding authors at: CAS Key Laboratory of Microscale Magnetic Resonance and Department of Modern Physics, University of Science and Technology of China, Hefei 230026, China (X. Peng) and National High Magnetic Field Laboratory, Florida 32310, USA (R. Fu).

E-mail addresses: xhpeng@ustc.edu.cn (X. Peng), rfu@magnet.fsu.edu (R. Fu).

https://doi.org/10.1016/j.jmr.2018.06.012
1090-7807/© 2018 Elsevier Inc. All rights reserved.

In this paper, we use AHT to obtain constraint equations and then solve such equations in order to select any desired Hamiltonians. We describe a general procedure using both flip-angle and phase of applied pulses as control variables to design multiple pulse sequences to achieve the desired average Hamiltonians from an achievable set of average sub-Hamiltonians in solid-state homonuclear NMR systems. In particular, constraint equations for homonuclear decoupling sequences were discussed, and two typical solutions were found: one for solid-echo based sequence and the other for a new homonuclear decoupling scheme. The remainder of the paper is organized as follows. In Section 2, a brief description of solid-state NMR systems and concept of multiple pulse sequences are given. In Section 3, the reachable set of average sub-Hamiltonians in solid-state NMR by AHT is derived theoretically and the general procedure of how to select any given sub-Hamiltonian is described. The performance of the newly derived homonuclear dipolar decoupling sequence is discussed experimentally in Sections 4 and 5.

2. Solid-state NMR and multiple pulse sequences

Let us consider a solid-state system of homonuclear spins I = 1/2 that are coupled through the dipolar interactions. In the usual rotating frame, the total Hamiltonian describing the nuclear spin system can be written as

$$H(t) = H_{CS} + H_D + H_{RF}(t), \tag{1}$$

where H_{CS} describes the offset resonance and chemical shift (CS) interactions, H_D represents the homonuclear dipolar interactions, and $H_{RF}(t)$ is the applied radio-frequency (RF) pulse. In high magnetic field for static solids,

$$H_{CS} = \sum_j (\Delta\omega + \omega_{cs}^j) I_z^j,$$

$$H_D = \sum_{j<l} \omega_D^{jl} (3 I_z^j I_z^l - \mathbf{I}^j \cdot \mathbf{I}^l), \tag{2}$$

$$H_{RF}(t) = \sum_j (\omega_{1x} I_x^j + \omega_{1y} I_y^j).$$

Here spin operators $\mathbf{I} = (I_x, I_y, I_z)$, $\Delta\omega$ is the frequency offset $\Delta\omega = \omega - \omega_0$, ω_{cs}^j is the chemical shift frequency, ω_D^{jl} is the dipolar constant between j and l spins, ω_{1x} and ω_{1y} denote the notation frequencies of the time-dependent RF field in the x and y directions.

A multiple pulse sequence [22] is illustrated in Fig. 1, where the kth pulse can be described by the operator $P_k = e^{-i\theta_k \mathbf{n}_k \cdot \mathbf{I}}$ with the flip angle θ_k along $\mathbf{n}_k$. Firstly, we study this multiple pulse sequence with δ-pulses, i.e., the evolutions during the pulses are neglected. Here the pulse sequence is limited to be cyclic with a cycle time $\tau_c = \sum_{k=1}^N \tau_k$, that is

$$\prod_{k=1}^{N} P_k = \mathbf{1}, \tag{3}$$

where $\mathbf{1}$ denotes the identity operator.

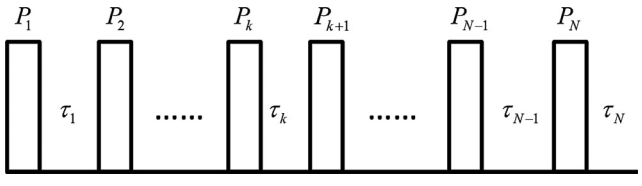

Fig. 1. Illustration of a multiple pulse sequence. Here P_k is the kth operator for the ideal pulse and τ_k are time intervals between pulses.

3. Theory

3.1. Average Hamiltonian theory

In order to understand the effect of the applied RF term on the internal spin Hamiltonians, we transform the total Hamiltonian into the interaction frame by the propagator

$$U_{RF}(t) = \mathcal{T}\exp\{-i\int_0^t dt' H_{RF}(t')\}, \tag{4}$$

where $\mathcal{T}$ is the Dyson time ordering operation. In the interaction representation, the system Hamiltonian becomes

$$\tilde{H}_S(t) = U_{RF}^\dagger(t) H_S U_{RF}(t), \tag{5}$$

where, $H_S = H_{CS} + H_D$. According to AHT, the zero-order average Hamiltonian over τ_C is given by $\bar{H}^{(0)} = \frac{1}{\tau_c}\int_0^{\tau_c} \tilde{H}_S(t)dt = \frac{1}{\tau_c}\sum_{k=1}^N \tilde{H}_{S,k}\tau_k$, where $\tilde{H}_{S,k}$ is the Hamiltonian during the kth interval in the interaction representation and can be expressed as:

$$\tilde{H}_{S,k} = \left(\prod_{k'=1}^{k} P_{k'}\right)^\dagger H_S \left(\prod_{k'=1}^{k} P_{k'}\right). \tag{6}$$

$P_{k'}$ is the global rotation of the spin, then we have

$$\prod_{k'=1}^{k} P_{k'} = R(\Omega_k) = R_z(\alpha_k) R_y(\beta_k) R_z(\gamma_k), \tag{7}$$

where $\Omega_k = (\alpha_k, \beta_k, \gamma_k)$ denotes the three Euler rotational angles due to the RF fields. By inserting these matrices into $\tilde{H}_{S,k}$, we get the following expression:

$$\tilde{H}_{S,k} = \sum_j (\Delta\omega + \omega_{cs}^j) I_{(\beta_k,\alpha_k)}^j + \sum_{j<l} \omega_D^{jl} (3 I_{(\beta_k,\alpha_k)}^j I_{(\beta_k,\alpha_k)}^l - \mathbf{I}^j \cdot \mathbf{I}^l). \tag{8}$$

Here, $I_{(\beta_k,\alpha_k)} = \sin\beta_k \cos\alpha_k I_x + \sin\beta_k \sin\alpha_k I_y + \cos\beta_k I_z$. This formula can be expanded as

$$\begin{aligned}\tilde{H}_{S,k} = &\sum_j (\Delta\omega + \omega_{cs}^j)[\sin\beta_k\cos\alpha_k I_x^j + \sin\beta_k \sin\alpha_k I_y^j + \cos\beta_k I_z^j] \\ &+ \sum_{j<l} \omega_D^{jl}\Big[\frac{3\cos^2\beta_k - 1}{2}(3 I_z^j I_z^l - \mathbf{I}^j\cdot\mathbf{I}^l) \\ &+ \frac{1}{2}\sin(2\beta_k)\cos\alpha_k (I_z^j I_x^l + I_x^j I_z^l) + \frac{1}{2}\sin(2\beta_k)\sin\alpha_k (I_z^j I_y^l + I_y^j I_z^l) \\ &+ \frac{1}{2}\sin^2\beta_k \cos(2\alpha_k)(I_x^j I_x^l - I_y^j I_y^l) \\ &+ \frac{1}{2}\sin^2\beta_k \sin(2\alpha_k)(I_y^j I_x^l + I_x^j I_y^l)\Big]\end{aligned} \tag{9}$$

Since $\tilde{H}_{S,k}$ is independent of γ_k, it can be denoted as $\tilde{H}_{S,k} = H(\alpha_k, \beta_k)$. With this notation, the internal Hamiltonian can be simply written as $H_S = H(0,0)$, and zero-order average Hamiltonian as $\bar{H}^{(0)} = \frac{1}{\tau_c}\sum_{k=1}^N [H(\alpha_k, \beta_k)\tau_k]$. By inserting the solution (α_k, β_k) into Eq. (7), we can achieve the overall rotation by the kth pulse in the multiple pulse sequence. Since γ_k does not contribute to $\tilde{H}_{S,k}$, it can be set to any value. Although there are many ways to implement P_k experimentally depending on the choice of γ_k, we can simply set $\gamma_k = -\alpha_k$, such that P_k can be expressed as a product of two rotation operations:

$$\begin{aligned}P_k &= R(\Omega_k) R^\dagger(\Omega_{k-1}) \\ &= R_z(\alpha_k) R_y(\beta_k) R_z(\gamma_k) R_z(-\gamma_{k-1}) R_y(-\beta_{k-1}) R_z(-\alpha_{k-1}) \\ &= R_{\alpha_k+\frac{\pi}{2}}(\beta_k) R_{\alpha_{k-1}+\frac{\pi}{2}}(-\beta_{k-1}),\end{aligned} \tag{10}$$

where $\Omega_0 = (0,0,0)$. In other word, the phase and flip-angle of the applied RF pulse can be considered as two independent control variables in the design of multiple pulse sequences.

3.2. A reachable set of average sub-Hamiltonians

Obviously, $\bar{H}^{(0)}$ is contained in the space spanned by a set of $\mathcal{S}$:

$$\mathcal{S} = \{H_{CS}^{X}, H_{CS}^{Y}, H_{CS}^{Z}, H_{D}^{Z}, H_{D}^{SQC_X}, H_{D}^{SQC_Y}, H_{D}^{DQC}, H_{D}^{ZQC}\}. \tag{11}$$

where

$$H_{CS}^{X} = \sum_{j}(\Delta\omega + \omega_{cs}^{j})I_{x}^{j}$$

$$H_{CS}^{Y} = \sum_{j}(\Delta\omega + \omega_{cs}^{j})I_{y}^{j}$$

$$H_{CS}^{Z} = \sum_{j}(\Delta\omega + \omega_{cs}^{j})I_{z}^{j}$$

$$H_{D}^{Z} = \sum_{j<l}\omega_{D}^{jl}(3I_{z}^{j}I_{z}^{l} - \mathbf{I}^{j}\cdot\mathbf{I}^{l})$$

$$H_{D}^{SQC_Y} = \sum_{j<l}\omega_{D}^{jl}(I_{z}^{j}I_{y}^{l} + I_{y}^{j}I_{z}^{l})$$

$$H_{D}^{SQC_X} = \sum_{j<l}\omega_{D}^{jl}(I_{z}^{j}I_{x}^{l} + I_{x}^{j}I_{z}^{l})$$

$$H_{D}^{DQC} = \sum_{j<l}\omega_{D}^{jl}(I_{x}^{j}I_{x}^{l} - I_{y}^{j}I_{y}^{l})$$

$$H_{D}^{ZQC} = \sum_{j<l}\omega_{D}^{jl}(I_{x}^{j}I_{y}^{l} + I_{y}^{j}I_{x}^{l})$$

Here, H_{CS}^{X}, H_{CS}^{Y}, and H_{CS}^{Z} are considered as chemical shift components along X, Y and Z, respectively; H_{D}^{Z} is the Zeeman order term, which does not affect the thermal equilibrium state; the single-quantum coherence terms $H_{D}^{SQC_X}$ and $H_{D}^{SQC_Y}$ flip one spin only, which can be used to create the odd-order coherence from thermal equilibrium state [9]; the double-quantum coherence term H_{D}^{DQC} flips both spins up and down together, which is the Hamiltonian used to create even-order coherences in multiple-quantum solid-state NMR spectroscopy [23–27]; The so-called zero-quantum coherence term H_{D}^{ZQC} simultaneously flips one spin up and another down and plays an important role in determining the proper zero-order functions [22].

It is obvious from Eq. (9) that each of these terms is manipulated differently by groups of two Euler rotational angles (α_k, β_k) induced by the RF pulses. Therefore, it is possible to design a specific pulse sequence such that the zero-order average Hamiltonian over a cycle period τ_C becomes

$$\bar{H}^{(0)} = \frac{1}{\tau_c}\sum_{k}H(\alpha_k, \beta_k)\tau_k \propto \xi, \tag{12}$$

here ξ is any term in the set of $\mathcal{S}$ (i.e. $\xi \in \mathcal{S}$). It is worth noting that when the number of the RF pulses in a cycle is small, the parameters (α_k, β_k) may not have enough variables to provide a solution for selecting any of these terms. Because there are eight elements in $\mathcal{S}$, while each pulse provides two variables, a minimum of four pulses is required to have a meaningful set of solutions. More RF pulses would provide more control variables such that more solutions could be found. In this article, four pulses with equal pulse intervals are considered for generality, so that the zero-order average Hamiltonian becomes:

$$\bar{H}^{(0)} \propto H(\alpha_1, \beta_1) + H(\alpha_2, \beta_2) + H(\alpha_3, \beta_3) + H(\alpha_4, \beta_4) = C\xi \tag{13}$$

where C is the coefficient, which is considered as a scaling factor for the given term ξ being selected.

As an example, if we want to select the H_{CS}^{Z} term only (i.e. the z-rotation), we can simply solve these constraint equations:

$$\begin{aligned}
&\sum_{k=1}^{4}\sin\beta_k e^{i\alpha_k} = 0\\
&\sum_{k=1}^{4}\frac{3\cos^2\beta_k - 1}{2} = 0\\
&\sum_{k=1}^{4}\frac{1}{2}\sin 2\beta_k e^{i\alpha_k} = 0\\
&\sum_{k=1}^{4}\sin^2\beta_k e^{i2\alpha_k} = 0.
\end{aligned} \tag{14}$$

It is important to note that both the flip-angle and phase of the applied pulses can be used as control variables to solve the above constraint equations, unlike in many multiple pulse sequences where the phases of the applied pulses were primarily used to design any specific averaging. One solution of (α_k, β_k) for selecting the H_{CS}^{Z} term can be easily obtained:

$$\alpha_k = \frac{k}{2}\pi, \beta_k = \theta_m, \tag{15}$$

where $\theta_m = 54.7^\circ$ is the magic angle and $k = 1, 2, 3, 4$, such that we have $\bar{H}^{(0)} = \frac{1}{\sqrt{3}}H_{CS}^{Z}$. In this case, the coefficient $C = \frac{1}{\sqrt{3}}$ is positive and we label C and (α, β) as C^+ and (α^+, β^+). Similarly, we label C and (α, β) as C^- and (α^-, β^-) when the coefficients are negative. In order to make $\bar{H}^{(0)} = -\frac{1}{\sqrt{3}}H_{CS}^{Z}$, we can simply set $\beta_k^+ = \pi + \beta_k^-$.

Analogously, possible solutions to select any term ξ in $\mathcal{S}$ while removing other terms are listed in Table 1, where the positive and negative scaling factors C^+ and C^- can be simply obtained by

Table 1
Solutions for (α_k, β_k) for selecting any given ξ while suppressing other terms.

ξ	α^+	β^+	C^+	α^-	β^-	C^-
H_{CS}^{Z}	$\alpha_k = \frac{k}{2}\pi$	$\beta_k = \theta_m$	$\frac{1}{\sqrt{3}}$	$\alpha_k = \frac{k}{2}\pi$	$\beta_k = \theta_m + \pi$	$-\frac{1}{\sqrt{3}}$
H_{CS}^{X}	$\alpha_1 = \alpha_2 = -\frac{1}{4}\pi$, $\alpha_3 = \alpha_4 = \frac{1}{4}\pi$	$\beta_k = (-1+(-1)^k)\frac{\pi}{2} + (-1)^k\theta_m$	$\frac{1}{\sqrt{3}}$	$\alpha_1 = \alpha_2 = -\frac{1}{4}\pi$, $\alpha_3 = \alpha_4 = \frac{1}{4}\pi$	$\beta_k = (3+(-1)^k)\frac{\pi}{2} + (-1)^k\theta_m$	$-\frac{1}{\sqrt{3}}$
H_{CS}^{Y}	$\alpha_1 = \alpha_2 = \frac{1}{4}\pi$, $\alpha_3 = \alpha_4 = \frac{3}{4}\pi$	$\beta_k = (-1+(-1)^k)\frac{\pi}{2} + (-1)^k\theta_m$	$\frac{1}{\sqrt{3}}$	$\alpha_1 = \alpha_2 = \frac{1}{4}\pi$, $\alpha_3 = \alpha_4 = \frac{3}{4}\pi$	$\beta_k = (3+(-1)^k)\frac{\pi}{2} + (-1)^k\theta_m$	$-\frac{1}{\sqrt{3}}$
H_{D}^{Z}	$\alpha_k =$ constant	$\beta_k = (1+(-1)^k)\frac{\pi}{2}$	1	$\alpha_k =$ constant	$\beta_k = (2+(-1)^k)\frac{\pi}{2}$	$-\frac{1}{2}$
$H_{D}^{SQC_X}$	$\alpha_1 = \alpha_2 = -\frac{1}{4}\pi$, $\alpha_3 = \alpha_4 = \frac{1}{4}\pi$	$\beta_k = (1+(-1)^k)\frac{\pi}{2} + \theta_m$	$\frac{2}{3}$	$\alpha_1 = \alpha_2 = \frac{3}{4}\pi$, $\alpha_3 = \alpha_4 = \frac{5}{4}\pi$	$\beta_k = (1+(-1)^k)\frac{\pi}{2} + \theta_m$	$-\frac{2}{3}$
$H_{D}^{SQC_Y}$	$\alpha_1 = \alpha_2 = \frac{1}{4}\pi$, $\alpha_3 = \alpha_4 = \frac{3}{4}\pi$	$\beta_k = (1+(-1)^k)\frac{\pi}{2} + \theta_m$	$\frac{2}{3}$	$\alpha_1 = \alpha_2 = -\frac{3}{4}\pi$, $\alpha_3 = \alpha_4 = -\frac{1}{4}\pi$	$\beta_k = (1+(-1)^k)\frac{\pi}{2} + \theta_m$	$-\frac{2}{3}$
H_{D}^{DQC}	$\alpha_1 = \alpha_2 = 0$, $\alpha_3 = \alpha_4 = \pi$	$\beta_k = (1+(-1)^k)\frac{\pi}{2} + \theta_m$	$\frac{2}{3}$	$\alpha_1 = \alpha_2 = \pi/2$, $\alpha_3 = \alpha_4 = 3\pi/2$	$\beta_k = (1+(-1)^k)\frac{\pi}{2} + \theta_m$	$-\frac{2}{3}$
H_{D}^{ZQC}	$\alpha_1 = \alpha_2 = \frac{1}{4}\pi$, $\alpha_3 = \alpha_4 = -\frac{3}{4}\pi$	$\beta_k = (1+(-1)^k)\frac{\pi}{2} + \theta_m$	$\frac{2}{3}$	$\alpha_1 = \alpha_2 = \frac{3}{4}\pi$, $\alpha_3 = \alpha_4 = -\frac{1}{4}\pi$	$\beta_k = (1+(-1)^k)\frac{\pi}{2} + \theta_m$	$-\frac{2}{3}$

changing either pulse phases or flip-angles. These solutions can be used as a basic building block for selecting any desirable sub-Hamiltonian ξ at zero-order averaging, while the odd-order averaging can be removed by introducing the reflection symmetry operations of the basic building block [12].

Therefore, a general way to engineer any desired Hamiltonian is: (1) Decompose the spin Hamiltonians into a linear combination of terms spanned in the set $\mathcal{S}$; (2) Solve the constraint equations to design a basic building block for any desired sub-Hamiltonian. As an example, by directly composing the basic building block for H_{CS}^{Z} and $-H_{CS}^{Z}$ with eight equally interleaved pulses where (α_k, β_k) satisfies these conditions:

$$\begin{cases} \alpha_k = \frac{k}{2}\pi, \beta_k = \theta_m, (k = 1,2,3,4) \\ \alpha_k = \frac{k-4}{2}\pi, \beta_k = \theta_m + \pi, (k = 5,6,7,8) \end{cases}, \tag{16}$$

all dipolar interactions as well as the chemical shift interactions will be vanished.

3.3. Application to homonuclear decoupling

3.3.1. Constraint equations for homonuclear decoupling sequences

The target of homonuclear decoupling is to remove the dipolar interactions, i.e.

$$\bar{H}_D^{(0)} = \frac{1}{\tau_c}\sum_{k=1}^{N}[\tilde{H}_{D,k}\tau_k] = 0. \tag{17}$$

Now we substitute Eq. (9) into this expression and obtain the following three constraint equations for homonuclear decoupling

$$\begin{cases} \sum_{k=1}^{N} \frac{3\cos^2\beta_k - 1}{2}\tau_k = 0, \\ \sum_{k=1}^{N} \sin(2\beta_k)e^{i\alpha_k}\tau_k = 0, \\ \sum_{k=1}^{N} \sin^2\beta_k e^{i2\alpha_k}\tau_k = 0. \end{cases} \tag{18}$$

with a total of 3 N unknown variables. If $N = 1$, no solution could be found; when $N > 1$, the solution is not unique because the number of variables is larger than the number of constraints. For simplicity in the multiple pulse sequence, we use the same interleaved delay τ_k between pulses. It is difficult to obtain all analytical solutions for the above constraint equations, but we can easily find two classes of solutions: (i) $\sin(2\beta_k) = 0$, (ii) $\cos^2\beta_k = 1/3$.

It is found that the common solid-echo based sequences belong to the class (i) as analyzed in Section 3.3.2, while the class (ii) leads to a new homonuclear decoupling scheme, as illustrated in Section 3.3.3.

3.3.2. Analysis of solid-echo based sequences

It is helpful for analyzing pulse cycles using similar notations as in the literature [6]. Solid-echo based sequences are a combination of basic solid-echo pulse pairs: $-R_x(\pi/2) - \tau - R_y(\pi/2) - \tau -$ [28] and are frequently used for decoupling purpose. The Hamiltonian during the intervals in the basic pulse pairs exists six possible states, namely $H(\frac{\pi}{2} \pm \frac{\pi}{2}, \frac{\pi}{2})$, $H(\pi \pm \frac{\pi}{2}, \frac{\pi}{2})$, $H(0, -\frac{\pi}{2} \pm \frac{\pi}{2})$ and can be written briefly as $H^{\pm X}, H^{\pm Y}, H^{\pm Z}$ here. In order to illustrate this notation, we consider WAHUHA [3] four pulse cycle as an example, one version of which can be written as $-\tau - R_x(\pi/2) - \tau - R_y(\pi/2) - \tau - R_y(0) - \tau - R_x(\pi/2) - \tau - R_y(\pi/2) - \tau -$, and the Hamiltonian during the interval can be written in short as $(H^Z, H^Y, H^X, H^X, H^Y, H^Z)$.

The β_k for all six possible states is either 0 or $\pi/2$, i.e., $\sin(2\beta_k) = 0$. Therefore, the solid-echo based sequences belong to the class (i) solution. In order to illustrate its decoupling performance, we calculated all terms in the set of $\mathcal{S}$ that are associated with the dipolar interaction during the delays in the sequence, as listed in Table. 2. In this table, the first row shows the value of (α, β, τ) in each delay, the other rows give the expansion coefficients of every term for the dipolar Hamiltonian $\tilde{H}$. Obviously the sum of the values in each row is zero, meaning that the dipolar interactions are removed at the zero-order averaging.

3.3.3. Derivation of a new scheme for homonuclear decoupling

For the class (ii) solution, since $\cos^2\beta_k = 1/3$, the constraint equations in Eq. (18) collapse into $\begin{cases} \sum_{k=1}^{N}\eta_k e^{i\alpha_k} = 0 \\ \sum_{k=1}^{N} e^{i2\alpha_k} = 0 \end{cases}$, here $\eta_k = \pm 1$ corresponds to $\sin(2\beta_k) = \pm\sqrt{2}/3$. A new homonuclear decoupling scheme can thus be designed as

$$\alpha_k = \frac{2k\pi}{N}, \beta_k = \theta_m. \tag{19}$$

Thus, one can design a sequence as:

$$R_{\frac{2\pi}{N}+\frac{\pi}{2}}(\theta_m) - \tau - R_{\frac{2\pi}{N}+\frac{\pi}{2}}(-\theta_m)R_{\frac{4\pi}{N}+\frac{\pi}{2}}(\theta_m) - \cdots - R_{\frac{2k\pi}{N}+\frac{\pi}{2}}(-\theta_m)R_{\frac{2(k+1)\pi}{N}+\frac{\pi}{2}}(\theta_m) - \cdots - R_{\frac{\pi}{2}}(\theta_m).$$

There are $N!$ permutations in the set $\{\frac{2\pi}{N}, \frac{4\pi}{N}, \cdots, \frac{2(N-1)\pi}{N}, 2\pi\}$, so that the $N!$ basic building blocks can be used to develop a series of cycles for removing the effects of the homonuclear dipolar interactions while preserving the off-resonance and chemical shift information. In this scheme, the zero-order average Hamiltonian is

$$\bar{H}^{(0)} = \bar{H}_{CS}^{(0)} = \frac{\sqrt{3}}{3}\sum_j(\omega + \omega_{CS}^j)I_z^j. \tag{20}$$

This sequence scales the chemical shift interactions by a factor of $1/\sqrt{3}$, which is the maximum scaling factor (SF) achievable in all homonuclear dipolar decoupling sequences in solid-state NMR spectroscopy [29]. Most importantly, the effective field for this sequence is along the Z direction, being considered as a Z-rotation operator.

From the constraint equations in Eq. (18), N = 3 is the minimal number for the case (ii) solution. Fig. 2 shows three new pulse cycles with $N = 3$, abbreviated as JJXXR3 sequences. Fig. 2a shows the basic building block. This sequence can only cancel the

Table 2
Calculation of the WAHUHA sequence.

(α, β, τ)	$(0,0,1)$	$(\pi/2, \pi/2, 1)$	$(0, \pi/2, 1)$	$(0, \pi/2, 1)$	$(\pi/2, \pi/2, 1)$	$(0,0,1)$
H_D^Z	1	−1/2	−1/2	−1/2	−1/2	1
$H_D^{SQC_y}$	0	0	0	0	0	0
$H_D^{SQC_x}$	0	0	0	0	0	0
H_D^{ZQC}	0	0	0	0	0	0
H_D^{DQC}	0	−1/2	1/2	1/2	−1/2	0

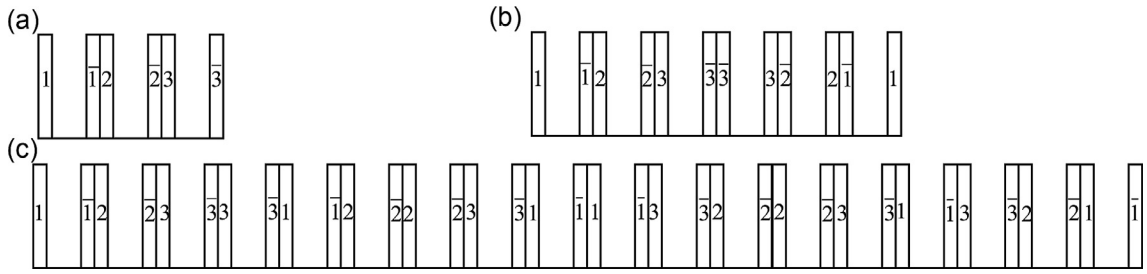

Fig. 2. Pulse sequences used for homonuclear dipolar decoupling. (a) JJXXR3-1; (b) JJXXR3-2; (c) JJXXR3-3. The vertical boxes in the sequences represent θ_p pulses of finite length τ_p. l and $\bar{l}$ denote the rotations of $R_{\frac{2l\pi}{3}+\frac{\pi}{2}}(\pm\theta_p)$, $(l = 1, 2, 3)$. The inter-pulse delay τ_{delay} should be optimized to compensate for the effect of finite pulse lengths in practical uses.

zero-order dipolar term under the δ-pulse assumption. The symmetric cycles in Fig. 2b remove the zero-order dipolar term and eliminate all odd-order terms over the entire cycle. The sequence in Fig. 2c is composed of six basic building blocks in such a way that the second-order dipolar term can be vanished, along the vanishing of all odd-ordered terms over a complete cycle due to the symmetric cycles.

In practice, the pulses are not ideal δ-pulses. Thus the effect of finite pulse length must be considered. If t_{pulse} and t_{delay} correspond to the total durations for the pulses and delays in the sequence, respectively, the total cycle time τ_C for the pulse sequence is $\tau_C = t_{pulse} + t_{delay}$. By adapting the method described in the literature [30], we can calculate the zero-order average Hamiltonian in the toggling frame during the pulses in the segment of $R_{\frac{2k\pi}{N}+\frac{\pi}{2}}(\theta_p) - \tau - R_{\frac{2k\pi}{N}+\frac{\pi}{2}}(-\theta_p)$. The obtained zero-order average Zeeman Hamiltonian is

$$\bar{H}^{(0)}_{CS,pulse} = \frac{\sin\theta_p}{\theta_p}\sum_j(\omega + \omega^j_{CS})I^j_z, \tag{21}$$

while the zero-order average homo-nuclear dipolar Hamiltonian becomes

$$\bar{H}^{(0)}_{D,pulse} = \frac{1}{4}H^Z_D + \frac{3\sin 2\theta_p}{8\theta_p}H^Z_D = \frac{1+3\mathrm{sinc}(2\theta_p)}{4}H^Z_D \tag{22}$$

Again, $H^Z_D = \sum_{j<l}\omega^{jl}_D(3I^j_zI^l_z - \mathbf{I}^j\cdot\mathbf{I}^l)$. On the other hand, the zero-order average dipolar Hamiltonian during the delays with flip-angle θ_p is

$$\bar{H}^{(0)}_{D,delay} = \frac{3\cos^2\theta_p - 1}{2}H^Z_D. \tag{23}$$

When $\theta_p = \theta_m = 54.7^\circ$, the zero-order average dipolar Hamiltonian becomes null during the delays but partially remains during the finite pulse lengths. Thus it cannot be canceled out over the entire cycle with the pulse flip-angle θ_m. In order to cancel the zero-order average dipolar Hamiltonian over the entire cycle in the presence of finite pulse lengths, the pulse flip-angle θ_p can be determined in such a way that

$$\begin{aligned}\bar{H}^{(0)}_D &= \frac{1}{\tau_c}[\frac{1+3\mathrm{sinc}(2\theta_p)}{4}t_{pulse} + \frac{3\cos^2\theta_p - 1}{2}t_{delay}]H^Z_D \\ &= DSF * H^Z_D\end{aligned} \tag{24}$$

Here, the dipolar scaling factor DSF is defined as

$$DSF = \frac{1}{1+DF}[A(\theta_p) * DF + B(\theta_p)], \tag{25}$$

where, $A(\theta_p) = \frac{1+3\mathrm{sinc}(2\theta_p)}{4}$, $B(\theta_p) = \frac{3\cos^2\theta_p - 1}{2}$, and the duty factor (DF) is defined as $DF = t_{pulse}/t_{delay}$. Clearly, when $DF = -B(\theta_p)/A(\theta_p)$, DSF = 0, meaning that the zero-order average homonuclear dipolar Hamiltonian over the entire cycle becomes null, while the zero-order average Zeeman Hamiltonian should remain along the Z direction having a scaling factor on chemical shift interactions

$$SF = \frac{\mathrm{sinc}\theta_p(-1 - 3\cos(2\theta_p)) + \cos\theta_p[1 + 3\mathrm{sinc}(2\theta_p)]}{-3\cos(2\theta_p) + 3\mathrm{sinc}(2\theta_p)} \tag{26}$$

Fig. 3 shows the plots of DF and SF as a function of the pulse flip-angle θ_p. Three interesting points should be noticed in the plots:

- When $t_{pulse} \ll t_{delay}$, which is the ideal case for δ-pulses, $\theta_p = 54.7^\circ$, the maximum SF of $1/\sqrt{3}$ is obtained.
- The maximum DF of 2.71 is found at $\theta_p = 105.9^\circ$ where SF = 0.31.
- The Zeeman term can be also cancelled (i.e. SF = 0) when $\theta_p = 120.3^\circ$.

Table 3 lists the average Hamiltonians and the properties (scaling factor and the overall tilt angle) of various homonuclear decoupling sequences. It can be seen from Table 3 that the newly designed JJXXR3-3 sequences appear to have a large scaling factor on chemical shift interactions while the average Hamiltonian is along the z axis, possessing the so-called Z-rotation. The WAHUHA sequence has a large scaling factor but the average Hamiltonian is along the direction tilted by 54.7° away the Z axis. Another sequence having such a Z-rotation is the MSHOT (magic sandwich high order truncation) sequence [31], which has a relatively small scaling factor on chemical shift interactions. Having the Z-rotation average Hamiltonian would simplify the setup of high-resolution two-dimensional (2D) heteronuclear correlation (HETCOR)

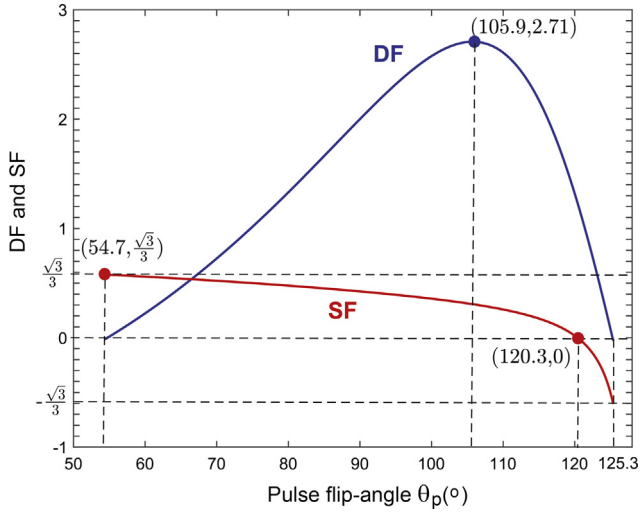

Fig. 3. Plots of SF and DF as a function of pulse flip-angle θ_p.

Table 3
Properties of Different Multiple Pulse Sequences.

Sequences	$\bar{H}_D^{(0)}$	$\bar{H}_D^{(1)}$	$\bar{H}_{CS,D}^{(1)}$	$\bar{H}_D^{(2)}$	SF	Tilt angle
JJXXR3-1	0	0	0	≠0	0.57*	0°
JJXXR3-2	0	0	0	≠0	0.57*	0°
JJXXR3-3	0	0	0	0*	0.57*	0°
WAHUHA [3]	0*	0	0*	≠0	0.57	54.7°
MREV-8 [5]	0	0	0*	≠0	0.47	45°
BR-24 [6]	0	0	0	0	0.38	54.7°
CORY-24 [4]	0	0	0	0	0.32	45°
MSHOT [31]	0	0	0	0	0.32	0°
FSLG [38]	0	≠0	≠0	≠0	0.57	54.7°

Note that: $\bar{H}_{CS,D}^{(1)}$ stands for the first-order cross term between Zeeman and dipolar interactions; Tilt angle corresponds to the direction of the average Hamiltonian with respect to the Z axis; Asterisks indicate the values obtained with the assumption of δ-pulses.

experiments [32]. In the next section, we apply these Z-rotation sequences in high-resolution 2D HETCOR experiments that correlate orientation-dependent, anisotropic ^{1}H chemical shifts in the t_1 dimension with ^{15}N chemical shifts in the t_2 dimension.

4. Experimental

All NMR measurements were carried out on a Bruker Avance 600 NMR spectrometer with Larmor frequencies of 600.13 and 60.82 MHz for ^{1}H and ^{15}N, respectively. The SPINAL decoupling sequence [33] with an ^{1}H RF amplitude of 62.5 kHz was used in all experiments during the ^{15}N detection in the t_2 dimension. ^{15}N and ^{1}H chemical shifts were referenced to the ^{15}N signal and water peak of an aqueous ^{15}N-labeled ammonium sulfate solution (5%, pH 3.1) at 0 and 4.7 ppm, respectively.

The HETCOR pulse sequence used in our experimental studies is shown in Fig. 4. In the t_1 dimension, the MSHOT and JJXXR3-3 sequences were applied as homonuclear decoupling block in the t_1 dimension to suppress the proton homonuclear interactions, a ^{1}H 90° pulse at the end of the t_1 dimension is applied to select the quadrature components using the States phase cycling in the t_1 dimension, followed by a short cross-polarization contact time, τ_{CP}, to ensure that the ^{15}N magnetization is the result of transfer from its closest ^{1}H. In the absence of the ^{15}N 180° pulse in the t_1 dimension, both the ^{1}H chemical shifts and the ^{1}H-^{15}N dipolar couplings are evolved, resulting in the ^{1}H-^{15}N dipolar splittings in the ^{1}H chemical shift dimension of the HETCOR spectra, the so-called dipolar-encoded HETCOR [32]. With a purple 180° ^{15}N pulse in the middle of the t_1 period, the ^{1}H-^{15}N heteronuclear dipolar coupling is refocused such that only the^{1}H chemical shifts are evolved, leading to typical ^{1}H-^{15}N HETCOR spectra.

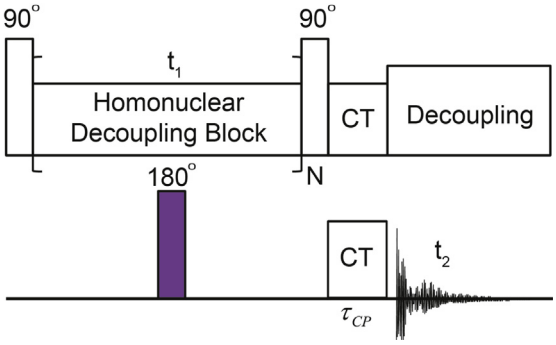

Fig. 4. HETCOR pulse sequence for ^{1}H–^{15}N correlation experiments. With 180 ^{15}N decoupling pulse (the purple pulse), the ^{1}H chemical shift is obtained in the ^{1}H dimension, while in the absence of the ^{15}N pulse, the ^{1}H–^{15}N dipolar splitting is shown in the ^{1}H dimension. The homonuclear decoupling sequence is applied in the t_1 dimension to remove the ^{1}H–^{1}H homonuclear dipolar interactions.

In order to determine the actual ^{1}H-^{15}N dipolar couplings, we first performed the typical ^{1}H-^{15}N HETCOR using the MSHOT homonuclear decoupling sequence in the presence of the ^{15}N 180° pulse in the middle of the t_1 period to remove the ^{1}H-^{15}N dipolar couplings, as shown in Fig. 5a (purple). A basic magic sandwich unit consists of τ_{delay}-$\tau_p(90°)\tau_p(360°)$ $\tau_p(360°)$ $\tau_p(90°)$ -τ_{delay}. In our experiments, τ_{delay} was set to 5.25 μs, and 90° and 360° pulse length τ_p were 3 and 12 μs, respectively. Two basic magic sandwich units were used as the t_1 increment in this experiment, which was 2x40.5 μs (=$2\tau_{delay}$+$2\tau_p(90°)$+$2\tau_p(360°)$), independent of the dwell time used in the acquisition parameter. Therefore, we can experimentally determine the dwell time in the acquisition parameter in such a way that any change in the ^{1}H offset can be correctly reflected in the ^{1}H chemical shift in the F1 dimension. For instance, once we obtained a HETCOR spectrum, we changed the ^{1}H offset by 2000 Hz in another experiment. If the scaling factor due to the MSHOT decoupling sequence is correctly compensated, we would expect that any ^{1}H resonance should shift by exactly the same amount of 2000 Hz. We could carefully adjust the dwell time in the acquisition parameter to fulfill this exactly same shift. In our experiments, when the dwell time was set to 28.26 μs, the ^{1}H resonance shifted by exactly the same amount. Thus, the experimentally determined scaling factor is 0.349 (=28.26 μs /81.0 μs). As shown in the HETCOR spectrum (purple, Fig. 5a) of ^{15}N-labeled acetyl-valine crystal sample, there are four magnetically nonequivalent ^{15}N resonances at 219.8, 187.8, 75.4, and 72.4 ppm in this given crystal orientation, and their bonded amide ^{1}H chemical shifts are 10.5, 12.8, 19.4, and 16.0 ppm, respectively.

5. Results and discussion

Fig. 5 displays the ^{1}H-^{15}N dipolar-encoded HETCOR spectra of ^{15}N-labeled acetyl-valine crystal sample using different decoupling schemes in the ^{1}H dimension. In the left side of each spectrum shows the corrected ^{1}H chemical shift scale (black), while in the right side (red) is the uncorrected chemical shift scale according to the actual t_1 increment used in the experiments, i.e. 81.0 μs for MSHOT and 28.7 μs for JJXXR3–3. As shown in Fig. 5a (black), for each ^{15}N resonance, the splitting along the ^{1}H chemical shift dimension represents the ^{1}H-^{15}N dipolar coupling, while the corresponding ^{1}H resonance is positioned at the center of the doublet. As indicated in the spectrum, the ^{1}H-^{15}N dipolar couplings are different for different ^{15}N resonances. This is because their amide ^{1}H-^{15}N bonds were oriented differently in the magnetic field at this crystal orientation. Thus, for the ^{15}N resonances at 219.8, 187.8, 75.4, and 72.4 ppm, the obtained ^{1}H-^{15}N dipolar couplings are 8.1, 7.4, 9.8, and 10.1 kHz, respectively.

Fig. 5b shows the dipolar-encoded HETCOR spectrum of the ^{15}N-labeled acetyl-valine crystal sample using the JJXXR3-3

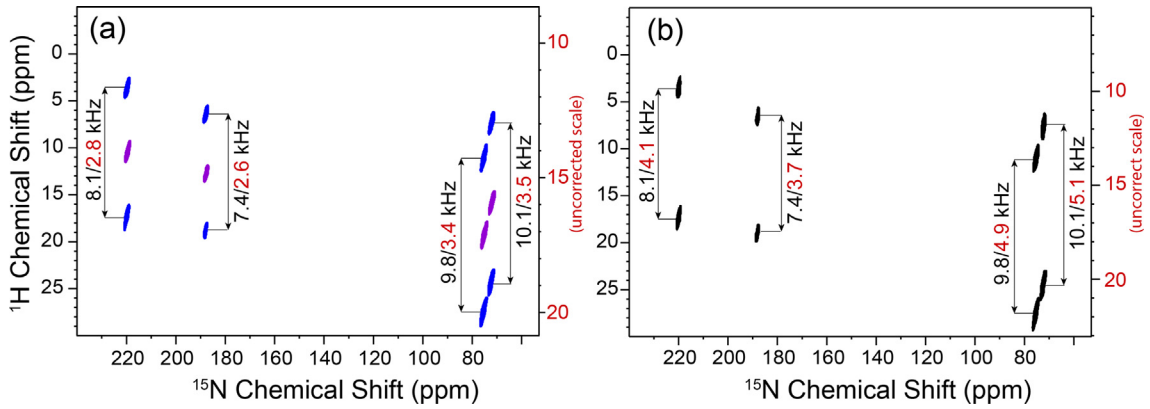

Fig. 5. Dipolar-encoded ^{1}H–^{15}N correlation spectra of ^{15}N-labeled acetyl-valine crystal sample using different decoupling schemes in the ^{1}H dimension. In these experiments, the ^{1}H carrier was set to 16.0 ppm. (a) MSHOT homonuclear decoupling, with (Purple) and without (Blue) ^{15}N 180° pulse in the middle of the ^{1}H dimension. Two basic magic sandwich units were used as the t_1 increment leading to the uncorrected scale (red) in the ^{1}H dimension in the right, while the chemical shift scale corrected using experimentally determined scaling factor is shown in black in the left side. (b) JJXXR3-3 homonuclear decoupling using a pulse flip-angle of 70 (τ_p = 2.33 μs) and a delay time τ_{delay} of 4.9 μs. The uncorrected chemical shift scale (red in the right) in the t_1 dimension was determined by a dwell time of 28.7 μs (=6τ_p + 3τ_{delay}, i.e. the cycle time for the basic unit in Fig. 2a). In the spectra, the corrected and uncorrected ^{1}H–^{15}N dipolar splittings are shown in black and red, respectively.

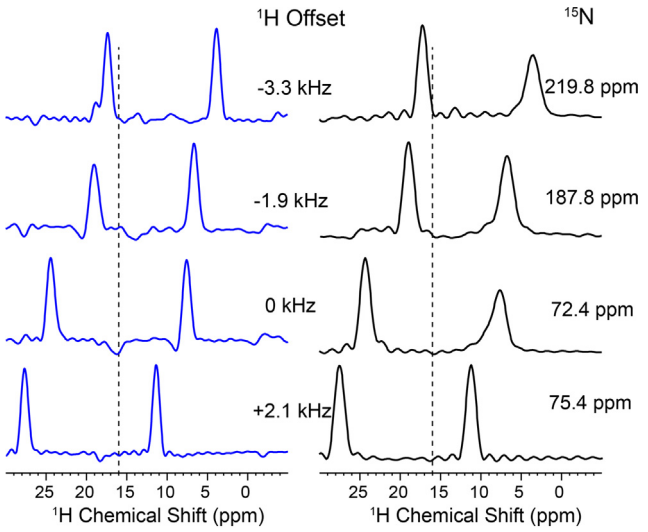

Fig. 6. Slices taken from the ^{15}N resonances at 219.8, 187.8, 72.4, and 75.4 ppm along the ^{1}H dimension from (Left) MSHOT and (Right) JJXXR3-3 in Fig. 5 showing the ^{1}H–^{15}N dipolar splittings at various ^{1}H offsets. The vertical dashed lines indicate where the ^{1}H carrier position was in the experiments.

homonuclear decoupling scheme shown in Fig. 2 with a pulse angle θ_p of 70° (τ_p =2.33 μs) and a delay time τ_{delay} of 4.9 μs. Since the dwell time was set to the total time period for the basic unit in Fig. 2a, i.e. 28.7 μs (=6τ_p+3τ_{delay}), we obtained the respective uncorrected ^{1}H-^{15}N dipolar couplings of 4.1, 3.7, 4.9, and 5.1 kHz for the ^{15}N resonances at 219.8, 187.8, 75.4, and 72.4 ppm. By comparing their actual ^{1}H-^{15}N dipolar couplings indicated in Fig. 5a, we could determine a scaling factor of 0.5 for this sequence with the pulse flip-angle of 70°, much larger than the scaling factor of 0.349 experimentally obtained in the MSHOT sequence.

Fig. 6 shows the slices taken at the ^{15}N resonances at 219.8, 187.8, 72.4, and 75.4 ppm along the ^{15}N dimension in Fig. 5. Since the ^{1}H carrier in our experiments was set to 16 ppm, the ^{15}N resonances at 219.8, 187.8, 75.4, and 72.4 ppm were irradiated under the decoupling at different ^{1}H offsets, which are the differences between the ^{1}H carrier position and their measured amide ^{1}H chemical shifts, corresponding to -3.3, -1.9, +2.1, and 0 kHz, respectively, as indicated in the spectrum. It is clear from Fig. 6 that both decoupling schemes have comparable ^{1}H–^{1}H homonuclear decoupling efficiency with ^{1}H offsets up to -3.3 kHz. It can also be noticed that the decoupling efficiency at positive ^{1}H offsets appears to be better than the negative offsets. In addition, it is important to note that the new JJXXR sequence has a much less DF than the MSHOT sequence. DF was 0.952 (=2τ_p/τ_{delay}) in this JJXXR3-3 decoupling sequence. While in the MSHOT experiment, DF was calculated to be 2.857 (i.e. =[τ_p(90°)+τ_p(360°)]/τ_{delay}) according to our experimental setup. In other words, the average ^{1}H decoupling power used in the JJXXR3-3 decoupling is about 30% less than in the MSHOT, but yielding a comparable decoupling efficiency. There is more potential in this regard in case when θ_p is small, as demonstrated in Fig. 3 where DF can be less with a smaller pulse flip-angle. As indicated in Table 3, the second-order average Hamiltonian $\bar{H}_D^{(2)}$ is vanished only when δ-pulses are used in the JJXXR3-3 sequence. Thus, it is anticipated that the JJXXR3-3 decoupling efficiency would be further improved with higher RF amplitude.

As indicated in Eq. (25), the zero-order average Hamiltonian can be achieved by adjusting the pulse flip-angle and the inter-pulse delay. As shown in Fig. 3, a smaller pulse flip-angle tends to give a larger scaling factor. When the pulse angle is about 120°, the projected scaling factor is close to zero. Fig. 7 shows the dipolar-encoded HETCOR spectra of the ^{15}N-labeled acetyl-valine crystal sample using the JJXXR3-3 homonuclear decoupling scheme at different pulse flip-angles. Clearly, the obtained ^{1}H-^{15}N dipolar splittings gradually became smaller with the increase of the pulse flip-angle. Fig. 8a shows the slices taken from the ^{15}N resonance at 75.4 ppm along the ^{1}H dimension from the spectra shown in Fig. 7. The measured uncorrected ^{1}H-^{15}N dipolar splitting was 5.36, 4.45, 3.05, and 0 kHz, corresponding to the scaling factor of 0.547, 0.454, 0.312, and 0, for the pulse flip-angle θ_p of 60°, 80°, 100°, and 120°, respectively. Fig. 8b shows the experimentally measured scaling factors at various θ_p, as predicted by Eq. (26). It can be noticed in Fig. 8a that the doublet at θ_p = 60° has broader line-widths as compared to the pulse flip-angles at 80° and 100°, suggesting that the homonuclear decoupling efficiency was compromised. This is owing to the fact that the total cycle time (i.e., 6τ_p+3τ_{delay}) for the basic unit was longer (33.6 μs at θ_p = 60° versus 26.68 μs at θ_p = 80°). However, the DF value was 0.556 at θ_p = 60°, even smaller than 0.952 at θ_p = 70°, indicating that the average decoupling power was lower. With 3 μs ^{1}H 90° pulse, the B_1 field used in our experiments was 83 kHz. In the MSHOT decoupling scheme, the average B_1 field for ^{1}H decoupling was 61.5 kHz (i.e.,

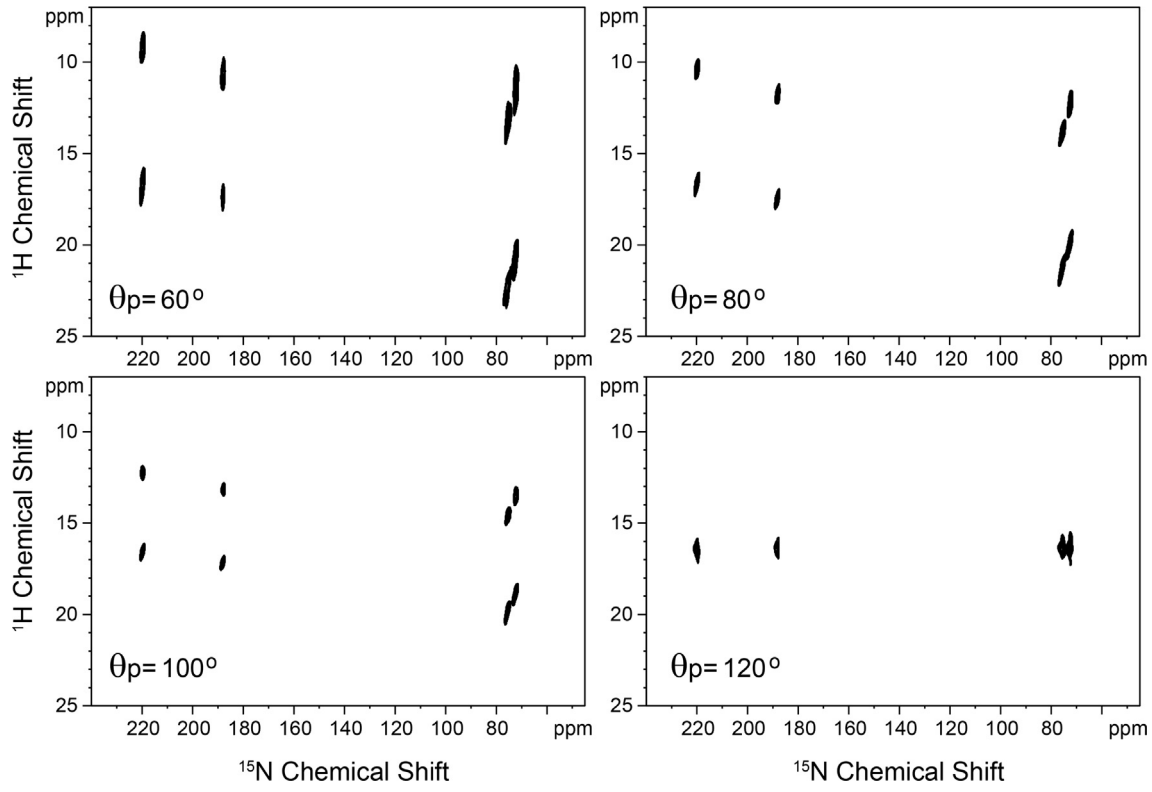

Fig. 7. Dipolar-encoded ^{1}H–^{15}N correlation spectra of ^{15}N-labeled acetyl-valine crystal sample using the JJXXR3-3 decoupling scheme with different pulse flip-angles. In our experiments, the pulse flip-angle was calculated based on the experimentally measured ^{1}H 180° pulse length of 6 μs, while the inter-pulse delay τ_{delay} was optimized to be 7.2, 3.9, 2.5, and 6.5 μs for the pulse flip-angle θ_p of 60°, 80°, 100°, and 120°, respectively. The uncorrected ^{1}H chemical shift scale is shown in all spectra.

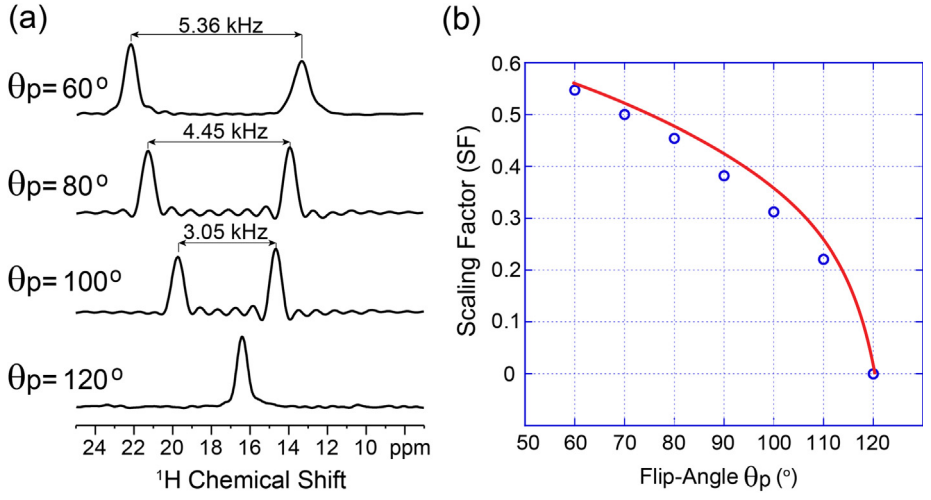

Fig. 8. (a) Slices taken from the ^{15}N resonance at 75.4 ppm along the ^{1}H dimension from the spectra shown in Fig. 7 showing the ^{1}H–^{15}N dipolar splittings at different pulse angles. (b) The experimentally obtained scaling factor at various pulse flip-angles in agreement with the predicted red curve from Eq. (26).

=83 kHz $*$ 2.857/(1 + 2.857)). While for the JJXXR3 decoupling scheme, the average B_1 field for ^{1}H decoupling became 40.5 kHz (i.e., =83 kHz $*$ 0.952/(1 + 0.952)) at $\theta_p = 70°$ and 29.7 kHz (i.e., =83 kHz $*$ 0.556/(1 + 0.556))at $\theta_p = 60°$. To improve the decoupling efficiency, we can simply reduce the ^{1}H 90° pulse length thus to shorten the total cycle time in the JJXXR3 scheme. Using such an efficient decoupling sequence with low average decoupling field would be a great help to prevent the RF heating in NMR experiments of hydrated biological samples [34].

The RF field inhomogeneity, which can be represented by the deviation ε of the pulse flip-angle across the sample region, is another factor that influences the decoupling efficiencies. As indicated in Eq. (24), averaging the zero-order dipolar Hamiltonian over the entire cycle in the basic unit of the JJXXR3 sequence is based on the cancelation of two dipolar components, one from the remaining dipolar interactions during the pulses and another one from during the delay, both of which are associated with the pulse flip-angle θ_p. In the presence of RF field inhomogeneity across the sample region, the pulse flip-angle becomes $(\theta_p + \varepsilon)$, the dipolar scaling factor in Eq. (25) becomes: $DSF(\theta_p + \varepsilon) = \frac{1}{1+DF}[A(\theta_p + \varepsilon) * DF + B(\theta_p + \varepsilon)]$, where DF = t_{pulse}/t_{delay} $= -B(\theta_p)/A(\theta_p)$, as the setting without pulse deviation. Fig. 9 shows

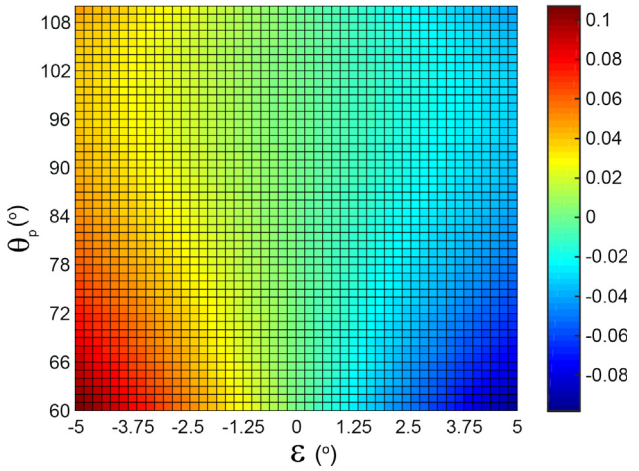

Fig. 9. Plot of DSF as a function of θ_p and ε. The color scale in the right represents the DSF values.

the plot of DSF$(\theta_p + \varepsilon)$ as a functions of θ_p and ε. It is apparent from Fig. 9 that the DSF value is small with a few degrees of pulse flip-angle deviation when θ_p is less than 110°, implying that the decoupling efficiency is insensitive to the RF field inhomogeneity. On the other hand, when θ_p is close to 120°, the DSF value increases quickly as ε increases (plot not shown), meaning that the decoupling efficiency becomes more sensitive to the RF field inhomogeneity. Typically, the RF field inhomogeneity can be compensated by constructing supercycles and designing symmetries in the pulse sequences [31,35–37]. Similarly, the symmetric cycles used in the JJXXR3-3 sequence could compensate the effect of the RF field inhomogeneity. As a matter of fact, with given pulse flip-angles, the JJXXR3-3 decoupling remained efficient even when the inter-pulse delay time τ_{delay} was varied by as large as 10% (spectra not shown), although the scaling factor on the chemical shift and heteronuclear ^{1}H-^{15}N dipolar coupling changed slightly.

Like many other homonuclear decoupling sequences [3–6], this decoupling sequence is designed to average the homonuclear dipolar interactions in the spin space where the time-dependent perturbation is introduced into the spin Hamiltonians through RF pulses. On the other hand, the spin Hamiltonians also become time-dependent when the sample is spinning, which may interfere with the time-dependent perturbation introduced into the spin Hamiltonians via RF pulses in the spin space. Typically, with the assumption of that the cycle time τ_C of a multiple pulse sequence is much shorter than the sample rotational period, it can be considered no interference takes place between them. In this regard, it appears that the frequency-switched Lee-Goldburg (FSLG) sequence [38] has the shortest τ_C among all available homonuclear decoupling sequences, thus it is simply applied when the sample spinning is fast. With the RF amplitude of 83 kHz (i.e. 90° pulse length of 3 μs) used in our experiments, τ_C for the basic unit of the JJXXR3 sequence was 28.7 μs (at $\theta_p = 70°$), which can hardly fulfill the above assumption even with a moderate spinning rate. In this case, the averaging in the spin space must be synchronized with the sample spinning in order to avoid destructive interference between the RF pulses and the sample spinning [14,39,40].

6. Conclusion

To conclude, we have theoretically derived a maximum achievable set of average Hamiltonians, each of which is manipulated differently by Euler angles induced by applied RF pulses, allowing us to design specific pulse sequences for selecting or engineering any given term from this set of the average sub-Hamiltonians. We have developed a general procedure using constraint equations where both flip-angle and phase of the applied pulses are used as control variables to select any of those sub-Hamiltonians. Using this procedure, we have successfully designed a novel homonuclear decoupling scheme using unconventional pulse flip-angles. It has been confirmed experimentally that this sequence effectively suppresses the ^{1}H–^{1}H homonuclear dipolar interactions and selects only the Iz term, meaning that the average Hamiltonian is along the Z direction, the so-called Z-rotation. Under the assumption of δ-pulses, this sequence has a maximum scaling factor of 0.57 on chemical shift and heteronuclear dipolar interactions. While with the finite pulse length, the scaling factor varies, depending on the flip-angles of the applied pulses. When the pulse flip-angle is close to 54.7°, this sequence possesses a large scaling factor with relatively low average decoupling field, as compared to the MSHOT sequence [31]. When the pulse angle becomes ∼120°, the scaling factor is almost zero, as if forming a "quadratic echo" [41] during which all interactions are refocused. We expect the general procedure developed here could be used in designing new pulse sequences to select any desirable Hamiltonian to obtain useful spectroscopic information and to achieve quantum logic gate controls in solid-state systems in the field of NMR quantum computation and simulation.

Acknowledgments

We thank Professor Dieter Suter for helpful discussions and comments. All NMR experiments were carried out at the National High Magnetic Field Lab (NHMFL) supported by the NSF Cooperative agreement no. DMR-1644779 and the State of Florida. This work is supported by National Key Basic Research Program of China (Grant Nos. 2014CB848700, 2018YFA0306600), the National Science Fund for Distinguished Young Scholars of China (Grants No. 11425523), the National Natural Science Foundation of China (Grants No. 11661161018), Anhui Initiative in Quantum Information Technologies (Grant No. AHY050000), Key Research Program of Frontier Sciences of the CAS (Grant No. QYZDY-SSWSLH004).

References

[1] E.L. Hahn, Spin Echoes, Phys. Rev. 80 (1950) 580–594.
[2] H.Y. Carr, E.M. Purcell, Effects of Diffusion on Free Precession in Nuclear Magnetic Resonance Experiments, Phys. Rev. 94 (1954) 630–638.
[3] J.S. Waugh, L.M. Huber, U. Haeberlen, Approach to High-Resolution nmr in Solids, Phys. Rev. Lett. 20 (1968) 180–182.
[4] D.G. Cory, A new multiple-pulse cycle for homonuclear dipolar decoupling, J. Magn. Reson. 94 (1991) 526–534.
[5] W.K. Rhim, D.D. Elleman, L.B. Schreiber, R.W. Vaughan, Analysis of multiple pulse NMR in solids, II. J. Chem. Phys. 60 (1974) 4595–4604.
[6] D.P. Burum, W.K. Rhim, Analysis of multiple pulse NMR in solids, III. J. Chem. Phys. 71 (1979) 944–956.
[7] M.H. Levitt, R. Freeman, Composite pulse decoupling, J. Magn. Reson. 43 (1981) 502–507.
[8] A.J. Shaka, J. Keeler, R. Freeman, Evaluation of a new broadband decoupling sequence: WALTZ-16, J. Magn. Reson. 53 (1983) 313–340.
[9] D. Suter, S.B. Liu, J. Baum, A. Pines, Multiple quantum NMR excitation with a one-quantum hamiltonian, Chem. Phys. 114 (1987) 103–109.
[10] U. Haeberlen, J.S. Waugh, Coherent Averaging Effects in Magnetic Resonance, Phys. Rev. 175 (1968) 453–467.
[11] W.K. Rhim, D.D. Elleman, R.W. Vaughan, Analysis of multiple pulse NMR in solids, J. Chem. Phys. 59 (1973) 3740–3749.
[12] M.H. Levitt, Symmetry in the design of NMR multiple-pulse sequences, J. Chem. Phys. 128 (2008) 052205.
[13] M.H. Levitt, R. Freeman, T. Frenkiel, Broadband heteronuclear decoupling, J. Magn. Reson. 47 (1982) 328–330.
[14] Y. Ishii, T. Terao, Manipulation of nuclear spin Hamiltonians by rf-field modulations and its applications to observation of powder patterns under magic-angle spinning, J. Chem. Phys. 109 (1998) 1366–1374.
[15] I.M. Georgescu, S. Ashhab, F. Nori, Quantum simulation, Rev. Mod. Phys. 86 (2014) 153–185.

[16] G.A. Alvarez, D. Suter, NMR quantum simulation of localization effects induced by decoherence, Phys. Rev. Lett. 104 (2010) 230403.
[17] X. Peng, J. Du, D. Suter, Quantum phase transition of ground-state entanglement in a Heisenberg spin chain simulated in an NMR quantum computer, Phys. Rev. A 71 (2005).
[18] X. Peng, J. Zhang, J. Du, D. Suter, Quantum simulation of a system with competing two- and three-body interactions, Phys. Rev. Lett. 103 (2009) 140501.
[19] Y.S. Weinstein, S. Lloyd, J. Emerson, D.G. Cory, Experimental implementation of the quantum baker's map, Phys. Rev. Lett. 89 (2002) 157902.
[20] J. Du, N. Xu, X. Peng, P. Wang, S. Wu, D. Lu, NMR implementation of a molecular hydrogen quantum simulation with adiabatic state preparation, Phys. Rev. Lett. 104 (2010) 030502.
[21] L.M.K. Vandersypen, I.L. Chuang, NMR techniques for quantum control and computation, Rev. Mod. Phys. 76 (2004) 1037–1069.
[22] M. Mehring, Principles of High Resolution NMR in Solids, Springer Verlag, 1983.
[23] R.F.A. Bax, S.P. Kempsell, Natural abundance carbon-13-carbon-13 coupling observed via double-quantum coherence, J. Am. Chem. Soc. 102 (1980) 4849–4851.
[24] A.P.J. Baum, Mutliple quantum dynamics in solid state NMR, J. Am. Chem. Soc. 108 (1986) 7447.
[25] W.S.V.Y. Ba, Multiple-quantum nuclear magnetic resonance spectroscopy of coupled 12 spins in solids combination with cross-polarization and magic-angle spinning, Solid State Nucl. Magn. Reson. 3 (1994) 249–269.
[26] A. Pines, Y.-S. Yen, Multiple-quantum NMR in solids, J. Chem. Phys. 78 (1983) 3579–3582.
[27] R. Tycko, Selection rules for multiple quantum NMR excitation in solids: derivation from time-reversal symmetry and comparison with simulations and C-13 NMR experiments, J. Magn. Reson. 139 (1999) 302–307.
[28] E. Vinogradov, P.K. Madhu, S. Vega, Strategies for high-resolution proton spectroscopy in solid-state NMR, Top. Curr. Chem. 246 (2005) 33–90.
[29] E. Salager, J.N. Dumez, L. Emsley, M.H. Levitt, A scaling factor theorem for homonuclear dipolar decoupling in solid-state NMR spectroscopy, J. Magn. Reson. 212 (2011) 11–16.
[30] D.P. Burum, M. Linder, R.R. Ernst, Low-power multipulse line narrowing in solid-state NMR, J. Magn. Reson. 44 (1981) 173–188.
[31] M. Hohwy, N.C. Nielsen, Elimination of high order terms in multiple pulse nuclear magnetic resonance spectroscopy: Application to homonuclear decoupling in solids, J. Chem. Phys. 106 (1997) 7571–7586.
[32] R. Fu, M. Truong, R.J. Saager, M. Cotten, T.A. Cross, High-resolution heteronuclear correlation spectroscopy in solid state NMR of aligned samples, J. Magn. Reson. 188 (2007) 41–48.
[33] B.M. Fung, A.K. Khitrin, K. Ermolaev, An improved broadband decouplingsequence for liquid crystals and solids, J. Mag. Reson. 142 (2000) 97–101.
[34] C. Li, Y. Mo, J. Hu, E. Chekmenev, C. Tian, F.P. Gao, R. Fu, P. Gor'kov, W. Brey, T.A. Cross, Analysis of RF heating and sample stability in aligned static solid-state NMR spectroscopy, J. Magn. Reson. 180 (2006) 51–57.
[35] P. Mansfield, M.J. Orchard, D.C. Stalker, K.H.B. Richards, Symmetrized multipulse nuclear-magnetic-resonance experiments in solids: measurement of the chemical-shift shielding tensor in some compounds, Phys. Rev. B 7 (1973) 90–105.
[36] W.-K. Rhim, D.D. Elleman, R.W. Vaugan, Enhanced resolution for solid-state, J. Chem. Phys. 58 (1973) 1772–1773.
[37] G.S. Boutis, P. Cappellaro, H. Cho, C. Ramanathan, D.G. Cory, Pulse error compensating symmetric magic-echo trains, J. Magn. Reson. 161 (2003) 132–137.
[38] W.I.G.M. Lee, Nuclear-magnetic-resonance line narrowing by a rotating rf field, Phys. Rev. 140 (1965) 1261–1271.
[39] S. Hafner, H.W. Spiess, Multiple-pulse assisted line-narrowing by fast magic-angle spinning, Solid State Nucl. Magn. Reson. 8 (1997) 17–24.
[40] D.E. Demco, S. Hafner, H.W. Spiess, Rotation-synchronized homonuclear dipolar decoupling, J. Magn. Reson. A 116 (1995) 36–45.
[41] M.M.M.A. Frey, J.N. VanHouten, K.L. Insogna, J.A. Madri, S.E. Barrett, Phosphorus-31 MRI of hard and soft solids using quadratic echo line-narrowig, PNAS 109 (2012) 5190–5195.